Application of Doppler Beam Sharpening for Azimuth Refinement in Prospective Low-THz Automotive Radars

IET Radar, Sonar & Navigation

Special Issue: Advanced Automotive Sensing – Towards Car Autonomy

IET Journals
The Institution of Engineering and Technology

Application of Doppler beam sharpening for azimuth refinement in prospective low-THz automotive radars

ISSN 1751-8784
Received on 12th March 2018
Revised 4th July 2018
Accepted on 18th July 2018
E-First on 11th September 2018
doi: 10.1049/iet-rsn.2018.5024
www.ietdl.org

Liam Daniel[1] ✉, Andrew Stove[1], Edward Hoare[1], Dominic Phippen[1], Mike Cherniakov[1], Bernie Mulgrew[2], Marina Gashinova[1]

[1]*Electronic, Electrical and Systems Engineering, University of Birmingham, Edgbaston, Birmingham, UK*
[2]*Institute for Digital Communications, The University of Edinburgh, Edinburgh, UK*
✉ *E-mail: l.y.daniel@bham.ac.uk*

Abstract: In this study, the authors investigate the application of the Doppler beam sharpening (DBS) technique for angular refinement to the emerging area of low-terahertz (THz) radar sensing. Ultimately this is to improve radar image quality in the azimuth plane to complement the excellent range resolution and thus improve object classification in low-THz radar imaging systems for autonomous platforms. The study explains the fundamental theory behind the process of DBS and describes the applicability of DBS to automotive sensing, indicating the potential for synthetic beamwidths of a fraction of a degree. Low-THz DBS was experimentally tested under controlled laboratory conditions, not only to accurately localised target objects in Cartesian space but also to provide unique object imaging at low-THz frequencies with wide azimuthal beamwidth antennas. It was shown that a stationary (i.e. non-scanned) wide beam antenna mounted on a moving platform can deliver imagery at least comparable to that produced by physical beamforming, be that steering arrays or narrow beam scanning antennas as in the experimental case presented.

1 Introduction

Recently there has been a surge in the requirement for the addition of increased autonomous features on vehicles, with the ultimate aim being full autonomy. This push has not only arisen due to the competition between motoring manufacturers but also from government, promoting the economic growth, increased road safety and efficiency that would come with being at the forefront of automotive autonomy development [1]. The introduction of the new European 4 GHz automotive band at 79 GHz [2], to complement the existing 77 and 24 GHz bands goes some way towards improving the diversity of automotive radar sensing [3]. However, in order to provide full autonomy and multi-functional capabilities, now is the right time to step from the traditional and rather rigid automotive sensor requirements and innovate. We must start looking at the development of novel techniques and configurations, which will ultimately lead to the development of the new generation of automotive sensing for autonomy.

Low-terahertz (THz) radar systems (0.1–1 THz) fit the requirements for future sensing for autonomous vehicles [4, 5]. Higher carrier frequencies provide inherently large bandwidths, giving very fine range resolutions. Additionally, as the wavelength λ decreases, an increased proportion of encountered scattering surfaces begin to appear rough [6]. This can be simply demonstrated by considering the Fraunhofer criterion for surface roughness: this states that a surface appears electromagnetically smooth provided the standard deviation of the surface roughness height h conforms to

$$h < \frac{\lambda}{32\cos\theta}, \tag{1}$$

where θ is the incidence angle of the electromagnetic wave to the surface. Therefore, with the frequency increase, scattering from rougher surfaces becomes more diffuse, less specular and backscatter is received from a fuller extent of an object, enabling more complete imaging of that object [7]. The shift to higher frequencies also has benefits for automotive manufacturers from a cost-space saving perspective, allowing for more compact components [8]. This includes smaller antennas able to deliver narrower beam widths, enabling higher angular resolutions. The rule of thumb relating antenna beamwidth θ_{bw} and physical dimension D is [9]

$$\theta_{\text{bw}} \propto \frac{\lambda}{D}, \tag{2}$$

indicating direct proportionality between antenna size and wavelength for a given required beamwidth.

The aforementioned fine range resolution and diffuse backscatter reflections at low-THz imply that much more information about an imaged scene may be obtained than with current mm-wave 77 GHz systems with moderate bandwidths (~200 MHz) and equally the 79 GHz standard. Low-THz frequencies will provide a future automotive radar system with extended capabilities – a radar able to produce high-quality imagery from real physical apertures, as opposed to only the gross object detection and velocity measurement provided by current adaptive cruise control systems. This enables the creation of a multi-functional radar system for path planning/passable region determination, on and off road feature and object identification capabilities and surface identification [10] for all weather on and off road autonomy. Examples of radar images measured at 150 GHz as part of an ongoing investigation into low-THz automotive imagery may be found in [4, 11].

While there are clear advantages to using low-THz frequencies, there is a common perception that high atmospheric and adverse weather attenuation will limit the effectiveness of low-THz radars. However, through careful positioning of the carrier frequency to lie between absorption peaks, the attenuation does not exceed 10 dB/km [12] and the operational range should satisfy the 200 m standard set for a ground based vehicles. Additionally, when considering attenuation due to rain, using the International Telecommunication Union Recommendation model for rain attenuation [13], we may expect an attenuation of around 11.4 dB/km at 77 GHz, 12.5 dB/km at 300 GHz and 10.8 dB/km at 1 THz for 25 mm/h rainfall. Experimentally the measured attenuation at 313 GHz was shown to be around 12 dB/km [14] and so it can be seen that the attenuation between low-THz and current 77 GHz

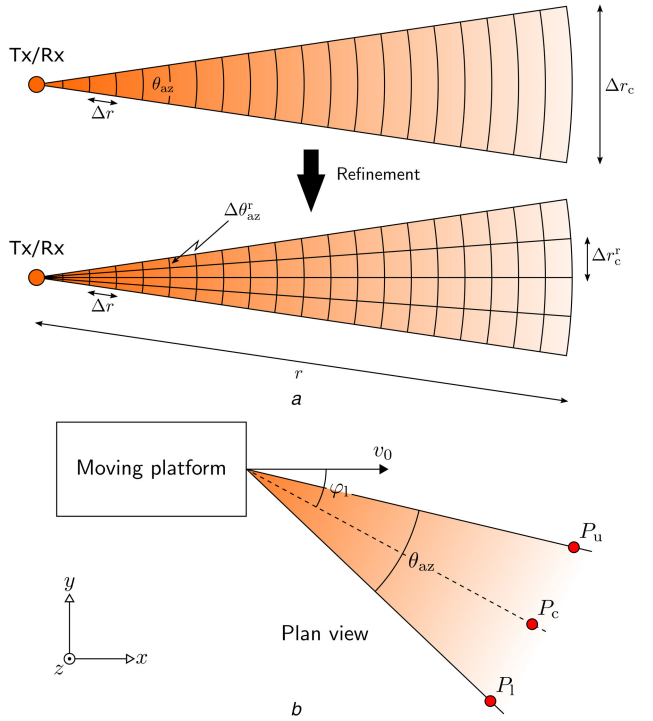

Fig. 1 *Azimuth refinement concept*

(a) Pictorial representation of the concept of azimuth refinement processing to improve angular (and cross range) resolution, ***(b)*** Moving platform scenario for DBS

automotive radars differs minimally. The same study showed that for 50 mm/h rainfall, the attenuation peaks at around 100 GHz and above this, remains constant or decreases. In [15], the authors have shown the results of measurements of attenuation in fog which demonstrated the little effect of fog on the imaging performance of the radar operating at 150 GHz.

The potential for high-resolution imaging with low-THz radars and the improvement available over current automotive radar technology motivates the research in the field. However, at longer ranges, image azimuth resolution of real aperture radar is degraded as cross-range resolution decreases in direct proportionality to the range – this results in a large disparity between the cross-range and range resolution. The degradation of image azimuth information would fundamentally affect any object classification effectiveness at longer ranges. It would also affect an autonomous vehicle's attempt to locate navigable free space. Even with very narrow (in terms of real aperture) scanned azimuthal antenna beam widths, θ_{az}, of the order of 1.5°, at a range of 70 m this provides a cross-range resolution, Δr_c, of $\simeq 1.8$ m. This value corresponds to the average vehicle width so that if any target was detected beyond such distance it would not be possible to determine if there is a path available for the vehicle to pass through.

To improve the cross-range resolution and enable operation at higher speeds, azimuth refinement is required to synthetically improve angular and cross-range resolutions. This study focuses on the use of Doppler beam sharpening (DBS) [16] for azimuth refinement.

DBS utilises the differences in the relative Doppler shift of targets at different angles with respect to a radar platform trajectory. An antenna beam may be synthetically partitioned into smaller angular sections by considering the difference in Doppler frequencies of the returns from across the beam width. Thus DBS is a technique that requires the radar platform to be in motion and for this motion to be known; it will not provide improved resolution for a stationary vehicle. The practical implementation of DBS for automotive purposes will be possible through the use of on-board inertial measurement units (IMUs) for vehicle motion estimation and localisation. The majority of research and application of DBS has been in airborne radar, where high velocities can lead to high-refinement factors. A summary of the development of DBS imaging in this context may be found in [17].

There are continuous advances made in this area of application, involving further improvement and adaptation of the DBS technique and applying super resolution methods for even greater refinement and image resolution [18–20]. The application of DBS for automotive purposes is less reported, there has, however, been research in the use of DBS for automotive height finding using 77 GHz frequency-modulated continuous-wave (FMCW) sensors [21]. This also introduces the use of the high-resolution spectral estimation technique called RELAX [22] to improve DBS resolution. The technique measured the height of a 4.5 m high entrance gate to an accuracy of 0.26 m (best case).

This study looks at the fundamental application of the DBS technique at low-THz frequencies for radar image azimuth enhancement. First, we look at the basic principles behind DBS and then discuss the applicability of DBS for use in automotive applications. Estimations of the potential azimuth resolution improvements that may be expected are made for some typical scenarios and parameters. Following this, experimental testing of DBS is discussed including a description of the experimental methodology, prototype low-THz radar systems, measurements conducted and the application of DBS signal processing. The measurements were made in controlled laboratory conditions and had two aims. First, to test the DBS processing using reference reflectors, examining the ability to resolve and locate a pair of corner reflector targets in Cartesian space. Secondly, to apply DBS in relation to the imaging of a complex target object. The experimental work was carried out at multiple frequencies as a proof of concept of the superior performance of DBS at low-THz frequencies, within the available testing constraints. Results of measurements of corner reflectors and target imaging are then presented and discussed.

2 Fundamentals of DBS

As described in Section 1, this work investigates the DBS form of azimuth refinement, for use in low-THz automotive radar. The goal is to synthetically increase the azimuth resolution and thus the cross-range resolution as depicted in Fig. 1*a*.

θ_{az} is the antenna physical azimuth beamwidth, Δr_c is the cross-range resolution at a given range from the radar transmitter/receiver (Tx/Rx). After refinement processing, the physical beamwidth is partitioned (refined) into finer angles $\Delta\theta^r_{az}$ (and thus cross-range resolution Δr^r_c). The range resolution Δr remains unchanged. In this section, we describe the DBS concept in its most fundamental form, purely in relation to azimuth resolution enhancement and following the general description as may be found in texts such as [23].

Fig. 1*b* shows a plan view of a moving sensor platform travelling with velocity v_0. The radar antenna of physical beam width θ_{az} is directed at a look angle of φ_l with respect to the platform motion. The points P_c, P_u and P_l lie (instantaneously) at the centre, upper and lower boundaries of the beam pattern, respectively.

The instantaneous Doppler of a target at point P_c, centred on boresight, is given by the monostatic Doppler equation [24]

$$f^c_d = \frac{2v_0 f_0}{c}\cos(\varphi_l), \tag{3}$$

where f_0 is the radar carrier frequency and c is the speed of light. The antennas finite beamwidth means that the instantaneous Doppler of targets at the beam extremities, points P_u and P_l, differ from this and are given by

$$\begin{aligned} f^u_d &= \frac{2v_0 f_0}{c}\cos\left(\varphi_l - \frac{\theta_{az}}{2}\right), \\ f^l_d &= \frac{2v_0 f_0}{c}\cos\left(\varphi_l + \frac{\theta_{az}}{2}\right). \end{aligned} \tag{4}$$

Thus, the spread in Doppler across the antenna beam due to the platform motion may be described by

$$\Delta f_{\mathrm{d}} = f_{\mathrm{d}}^{\mathrm{u}} - f_{\mathrm{d}}^{\mathrm{l}} = 2\frac{v_0 f_0}{c}\left[\cos\left(\varphi_{\mathrm{l}} - \frac{\theta_{\mathrm{az}}}{2}\right) - \cos\left(\varphi_{\mathrm{l}} + \frac{\theta_{\mathrm{az}}}{2}\right)\right]. \quad (5)$$

From a signal processing point of view, the Doppler spread spectrum will be split into a certain number of bins defined by the potential coherent integration time, τ. For a given integration time, the Doppler bin width is

$$\Delta f_{\mathrm{bin}} = \frac{1}{\tau}. \quad (6)$$

The number of Doppler bins n within the Doppler spread across the antenna pattern is therefore given by

$$n = \frac{\Delta f_{\mathrm{d}}}{\Delta f_{\mathrm{bin}}} = 2\frac{v_0 f_0 \tau}{c}\left[\cos\left(\varphi_{\mathrm{l}} - \frac{\theta_{\mathrm{az}}}{2}\right) - \cos\left(\varphi_{\mathrm{l}} + \frac{\theta_{\mathrm{az}}}{2}\right)\right] = 4\frac{v_0 f_0 \tau}{c}\sin(\varphi_{\mathrm{l}})\sin\left(\frac{\theta_{\mathrm{az}}}{2}\right) \quad (7)$$

with the constraint that $\varphi_{\mathrm{l}} \geq \theta_{\mathrm{az}}/2$ to ensure no Doppler ambiguity from targets either side of the platform motion vector. Fundamentally the DBS process is the mapping of the Doppler frequency to the azimuth angle, which is accomplished by rearrangement of (3)

$$\varphi_i = \arccos\left(\frac{c f_{\mathrm{d}}^i}{2 v_0 f_0}\right); \quad i = 1{:}n, \quad (8)$$

where φ_i is the refined azimuthal 'look' angle measured from the direction of motion, inferred from the Doppler frequency f_d^i of the ith frequency bin. It should be noted that any calculated $n < 1$, will have an artificially imposed lower limit of 1, which is the case of no resolution enhancement; limiting us to the original beam width defined azimuth resolution. The factor n is also known as the refinement factor, i.e. the factor by which azimuth and cross-range resolutions are improved. It can be seen from (7) that the refinement factor diminishes as the antenna becomes more forward looking, i.e. $\varphi_{\mathrm{l}} \to 0$. Relating back to Fig. 1*a*, the average refined azimuth $\Delta\theta_{\mathrm{az}}^{\mathrm{r}}$ and average cross-range resolutions $\Delta r_{\mathrm{c}}^{\mathrm{r}}$ over the antenna beam width are given by

$$\Delta\theta_{\mathrm{az}}^{\mathrm{r}} = \frac{\theta_{\mathrm{az}}}{n}, \quad \Delta r_{\mathrm{c}}^{\mathrm{r}} \simeq \frac{\Delta r_{\mathrm{c}}}{n}. \quad (9)$$

The dependence on carrier frequency is what actually motivates the use of the higher carrier, low-THz, frequencies to achieve resolution enhancement in a more forward looking scenario; assuming all other parameters are equal.

It should be noted that the azimuth enhancement is not evenly distributed over the antenna beam width (due to the cosine relationship between azimuth angle and Doppler), this is especially true for look angles close to 0° and with wider azimuth beam antennas.

Using this fundamental description of the angular improvements available through the use of DBS, the next section takes some example parameters in the context of automotive radar. This is to provide an indication of the applicability of DBS to automotive use and the imaging enhancement potential.

3 Potential modalities and application of DBS for automotive sensing

To consider the modalities and applicability of low-THz DBS to the automotive (autonomous driving) scenario, we provide examples of the potential azimuth refinements in some representative scenarios using representative values. The examples include investigation of existing automotive frequencies (77 and 24 GHz) as well as potential low-THz frequencies.

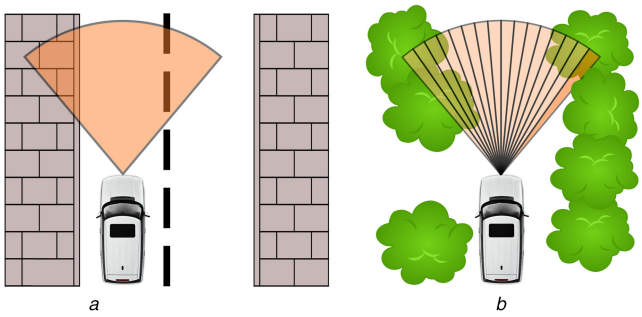

Fig. 2 *Two antenna configurations for the use of DBS*
(a) Using floodlight illumination and refinement of wide beam width, ***(b)*** Narrow beam scanning and refinement within the narrower beam

In general, an autonomous vehicle requires full 360° azimuth imaging, the focus here, however, is on estimating the potential to use DBS in a forward-looking system. The forward looking direction poses greater limits on azimuth resolution improvement as shown in Section 2; however, this direction requires possibly the highest resolution imaging for detection of potential hazards ahead.

Two antenna schemes are considered in this analysis, each with its own advantages – they are highlighted in Fig. 2. Fig. 2*a* shows a wide beam 'floodlight' type illumination of a large area in front of the vehicle, Fig. 2*b* shows a narrow beam illumination of multiple sectors ahead of the vehicle (equating to a total scan arc of the same azimuth extent as the floodlight). The latter may take the form of either a scanned beam or multi-beam staring, in either case, DBS is performed within each individual beam sector.

Multi-beams may provide an increased integration time, not being affected by scan dwell time. The scanned and multi-beam setups would enable a more flexible system, allowing for real aperture imaging when the vehicle is stationary. The wide beam 'floodlight' mode would require a smaller form factor antenna and reduced hardware complexity.

To make some practical estimates of azimuth refinement potential, the vehicle speeds to be used range between low speed off road crawl (5 mph/2.2 m/s) and motorway driving (70 mph/31.3 m/s). The overall angular sector of the region of interest ahead of the vehicle may be considered as ± 40° either side of forward looking, this fits with short- to mid-range modes of current commercial automotive radars [25]. Such a beam/scan arc would allow the detection of a pedestrian stepping from an offside kerb of an average 3.5 m wide UK road at a distance of ~6.25 m ahead of the vehicle (i.e. emerging from behind an obstruction on to the road). To make an informed estimate of the available integration time, commercial automotive radar specifications indicate an update rate in the order of 10 Hz [25]. This gives an integration time in the order of 0.1 s.

Fig. 3 shows the estimates of the refinement factors available for the chosen parameters above as a function of 5 frequencies: 24, 77 GHz (automotive standards), 150, 300 and 670 GHz. The highest three frequencies are considered low-THz and are chosen to be within low atmospheric attenuation bands [12, 26]. Fig. 3*a* shows the refinement factors relating to the wide beam 40° 'floodlight' illumination set at a look angle of 20° (i.e. one side of the full forward looking ±40°) – the inset shows a zoom of the refinement at the lower speeds. All frequencies give refinement across the beam, ranging from 8 to 230 times (24–670 GHz) at the lowest speed and from 117 to 3273 times at the highest. Practically these very high refinements may be unattainable and the plots do not show the refinement's angular distribution over the beam; however, the benefits of using low-THz frequencies are obvious. Figs. 3*b* and *c* show the refinement factors available to a narrow beam of 1.5° azimuth, covering the range of look angles equivalent to the 40° wide beam. This is for low-speed crawl (Fig. 3*b*) and high-speed motorway driving (Fig. 3c). Fig. 3*b* shows that in this mode, at low speeds, there would actually be no refinement possible at all in the current automotive bands and low-THz frequencies are absolutely necessary – low-speed angular refinement is possible at look angles > 4°. Fig. 3*c* shows that at the

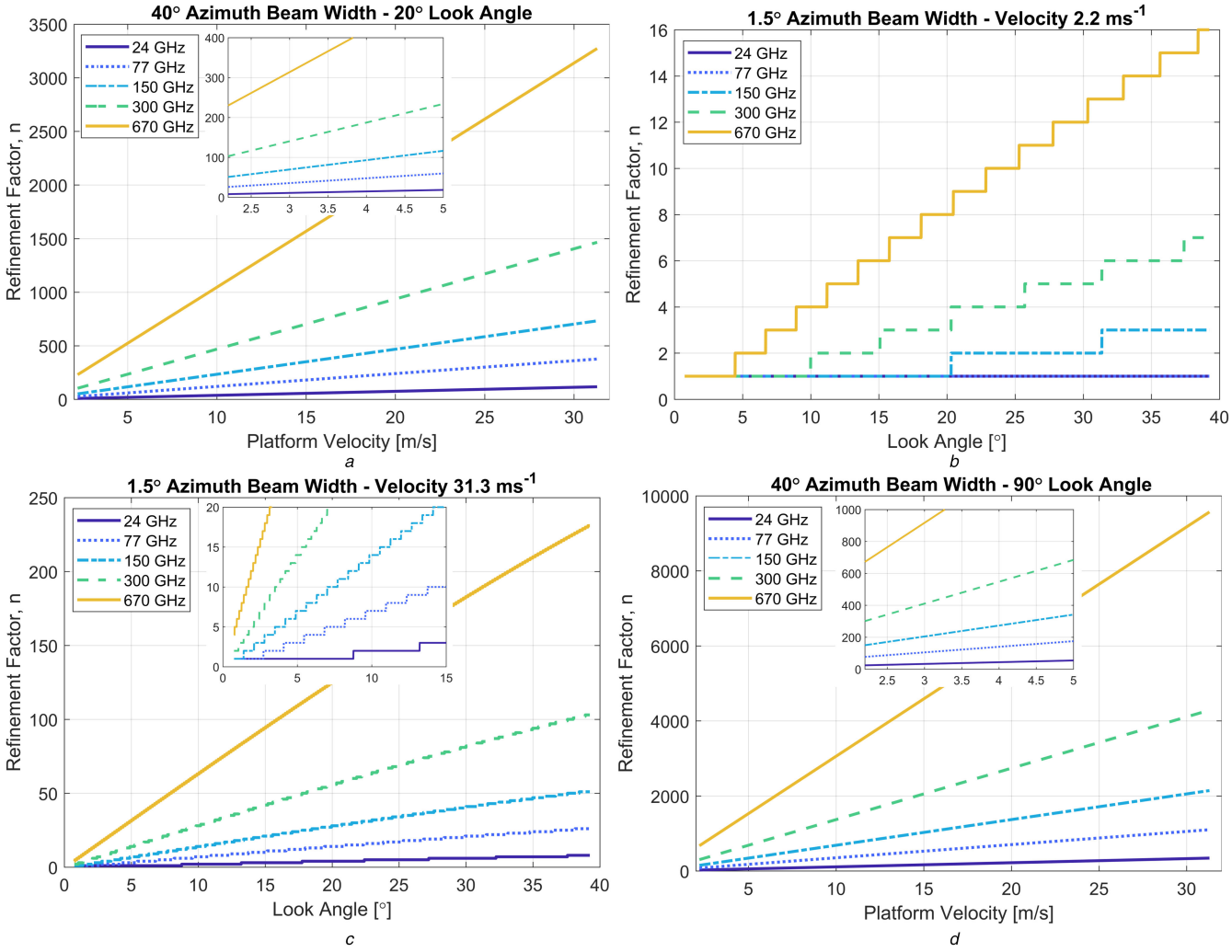

Fig. 3 *Refinement factors relating to real automotive parameters at different carrier frequencies*

(a) Wide beam forward looking refinement as a function of velocity, ***(b), (c)*** Refinement within a narrow beam width as a function of look angle at low- and high–speed, respectively, ***(d)*** Side looking wide beam refinement as a function of velocity

highest speed, refinement is even possible at the smallest look angle (0.75˚) for the 300 and 670 GHz, giving a refinement factor of 2 and 4, respectively. At a look angle of only 1.5˚ the 670 GHz frequency would enable a nine times refinement of the 1.5˚ antenna. These refinement factors indicate the potential for sub-degree synthetic beam widths, whilst at the current automotive frequency (77 GHz) the beam width would remain unchanged. It should be noted that there will be a trade-off between platform velocity and required azimuth refinement (and indeed integration time). This is based on the obstacles approach speed and distance (time) until collision and is a subject for further study.

As a matter of interest, Fig. 3*d* shows the large refinement factors available for the side looking case of the 40˚ beamwidth antenna, as a function of velocity. Although not useful for obstacle avoidance ahead of the vehicle, such enhanced images would be very useful for connected cars [27] where imaging data could be remotely passed to and used by the following vehicle.

The presented analysis has shown that there is good potential for azimuth refinement through DBS using low-THz frequencies. The near forward looking refinement may be low, but nevertheless exists at the highest frequencies and increases rapidly as look angle is increased – and we need to stress that any increase in angular resolution may be deemed beneficial. This, coupled with the fact that the fundamental application of DBS is relatively simple, motivates the study of low-THz DBS for automotive purposes.

Although not the focus for this study, it should be noted that in the automotive environment we may expect influence of the common issues of range and Doppler walk during the integration time, as well as the effect of moving targets and the requirement for motion compensation for a manoeuvring platform; these are unaccounted for in the basic DBS processing. These are the areas of future research for low-THz automotive DBS and techniques to deal with some of these issues are known in the literature for other system topologies, mainly related to aircraft-based DBS, e.g. [17, 28, 29]. However, it will be required that we develop and refine algorithms specific to our automotive scenario. As an example, due to the high bandwidths of low-THz radars, we may expect to compensate for substantial range walk. For a (conservative) 5 GHz bandwidth system, the mono-static range resolution is $\simeq 3$ cm. Thus, in the near forward direction, for a platform travelling at 30 mph (13.4 m/s) over an integration time of 0.1 s, we may expect a target to move through 45 range cells or 32 range cells at a look angle of 45°.

The next section of this paper is related to the experimental investigation of DBS at low-THz frequencies in order to verify the DBS algorithm application, processing, and imaging potential.

4 Experimental testing of DBS at low-THz frequencies

At this stage of the investigation, low-THz DBS is being tested under controlled laboratory conditions. Measurements are made at 79, 150 and 300 GHz for comparison. To provide the required Doppler shift for DBS, the radar platform motion is provided by a 2 m long linear positioner with accurate velocity and position control. The full experimental setup is shown in Fig. 4*a* and *b*. The radar platform has a maximum velocity and maximum acceleration/deceleration of 2.5 m/s and 2.5 m/s^2, respectively. In all experimentation, the acceleration and deceleration at the start

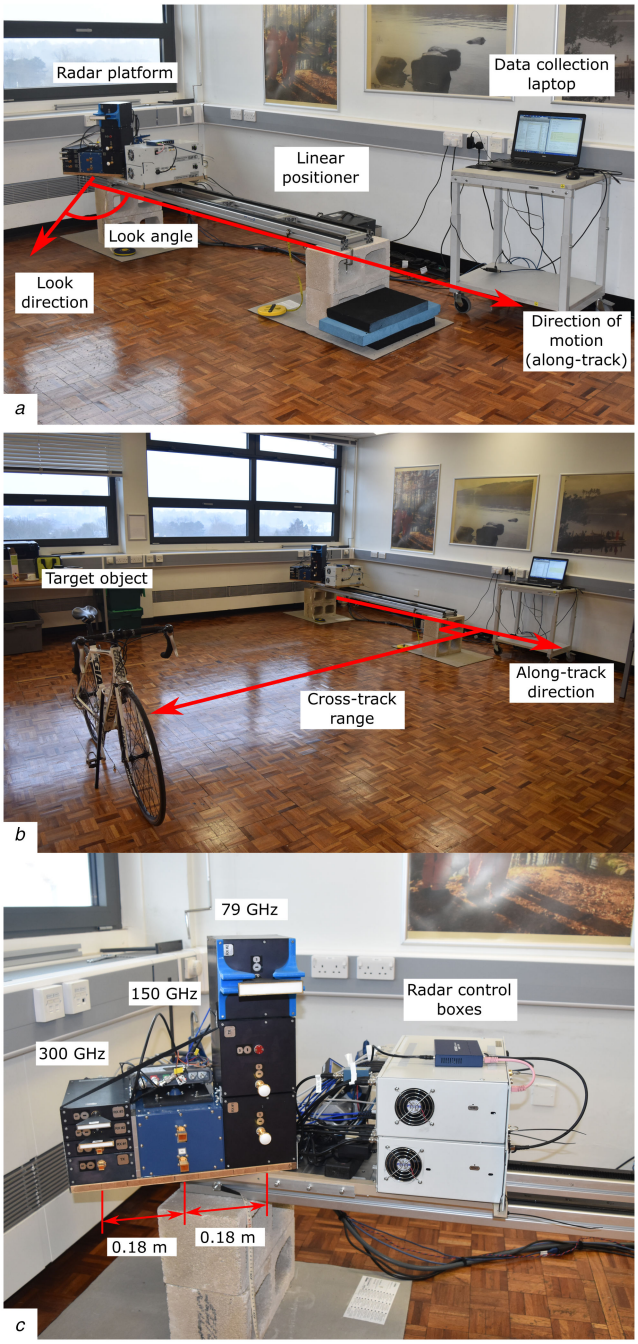

Fig. 4 *General experimental setup for DBS measurements*
(a) Shows the linear positioner with radar platform attached, ***(b)*** Shows the target object position and cross-track range, ***(c)*** 300 GHz, 150 and 79 GHz radar systems and their control boxes mounted on a linear positioner platform

and end of motion were maximal to reduce the duration of non-constant platform velocity. The radars are positioned pointing at the required look angle with respect to the along-track direction of motion of the linear positioner platform. Targets are placed within the setup at the required along-track and cross-track positions, platform motion and radar data collection are initiated from a laptop.

4.1 Prototype low-THz radar systems

The low-THz measurement systems used are bespoke prototype 79, 150, and 300 GHz FMCW radars; shown in Fig. 4*c*. These radars have the configurable bandwidth, centre frequency and chirp durations – the parameters used in the experimentation are found in Table 1.

The 300 GHz radar has a maximum bandwidth of 20 GHz, though for comparison of measurement, all radars, where possible, were set to a bandwidth of 5 GHz. Both 79 and 300 GHz systems have multiple receive units for use in 3D imaging and height finding [30]. The radars each have two different sets of similar beam pattern antennas. The first set is used for physical aperture imaging, with the antennas having a narrow two-way azimuthal beamwidth of $\simeq 1.2^{\circ}$ and wider elevation beamwidth of $\simeq 15^{\circ}$. The second set used in this experimentation in order to demonstrate the refinement process due to the DBS within the laboratory was a set of equal azimuth and elevation antennas with $\simeq 10^{\circ}$ beamwidth. This gives a measured two-way main lobe pattern of $\simeq 7.2^{\circ}$. The radar antenna centres are separated by 0.18 m horizontally, as shown in Fig. 4*c*.

As the radar traverses along the linear positioner, the chirps are emitted at the chirp repetition rate. The output waveforms are de-ramped baseband beat frequency data.

Table 1 Operational parameters of 79, 150, and 300 GHz FMCW radar

Parameter	Value		
centre frequency, GHz	79	148	290
bandwidth, GHz	5	6	5
range resolution, cm	3	2.5	3
chirp duration, ms	1	1	1
chirp repetition interval, ms	4.3	11.8	4.3
quadrature (I/Q) output	yes	yes	no

4.2 Experimental considerations and chosen experimental parameters

Considerations had to be made regarding the experimental setup, based around radar parameters, achieving best angular refinement and laboratory physical size. The first consideration was to look at the expected Doppler frequency spreads expected due to the platform motion and given antenna beamwidth. Due to the fact that the current experimental prototype has the limited chirp repetition rate, there is a potential for Doppler aliasing. In fact, a 300 GHz automotive radar would require around a 60 kHz maximum unambiguous Doppler to measure a target travelling radially at motorway speeds of 70 mph.

Fig. 5 shows the Doppler spread as a function of look angle and velocity for (Fig. 5*a*) 79 GHz, (Fig. 5*b*) 150 GHz and (Fig. 5*c*) 300 GHz radars. The horizontal black lines on the plots indicate the aliasing bands along with their corresponding aliasing factors. It is clear that at the higher frequencies and higher radar platform velocities aliasing may occur. If the aliasing factor N is known it is possible to recalculate the true frequency f_{t} from the measured aliased frequency f_{a} through the use of

$$f_{\mathrm{a}} = f_{\mathrm{t}} - Nf_{\mathrm{s}}, \tag{10}$$

for quadrature waveforms, where f_{s} is the chirp repetition rate. For the non-quadrature 300 GHz radar it is also required to know whether the expected Doppler is in the upper or lower part of an aliasing band (shown by dashed black horizontal lines in Fig. 5*b*). This is due to the additional presence of frequency folding. The true frequency can then be recalculated using

$$f_{\mathrm{a}} = |f_{\mathrm{t}} - Nf_{\mathrm{s}}|. \tag{11}$$

Due to the room size constraints and the Doppler spread and aliasing considerations, the look angle was chosen to be 60°. This angle allowed the Doppler spreads from many platform velocities to fit within the defined aliasing bands and also provided reasonable Doppler spread for azimuth refinement. In this situation, all possible measurements at 79 GHz are un-aliased. A platform velocity of 0.1 m/s was chosen to reduce the need to compensate for aliasing in the 300 GHz radar, but again still provide some level of Doppler spread. The 150 GHz radar then functions in the first aliasing band due to its lower chirp repetition rate.

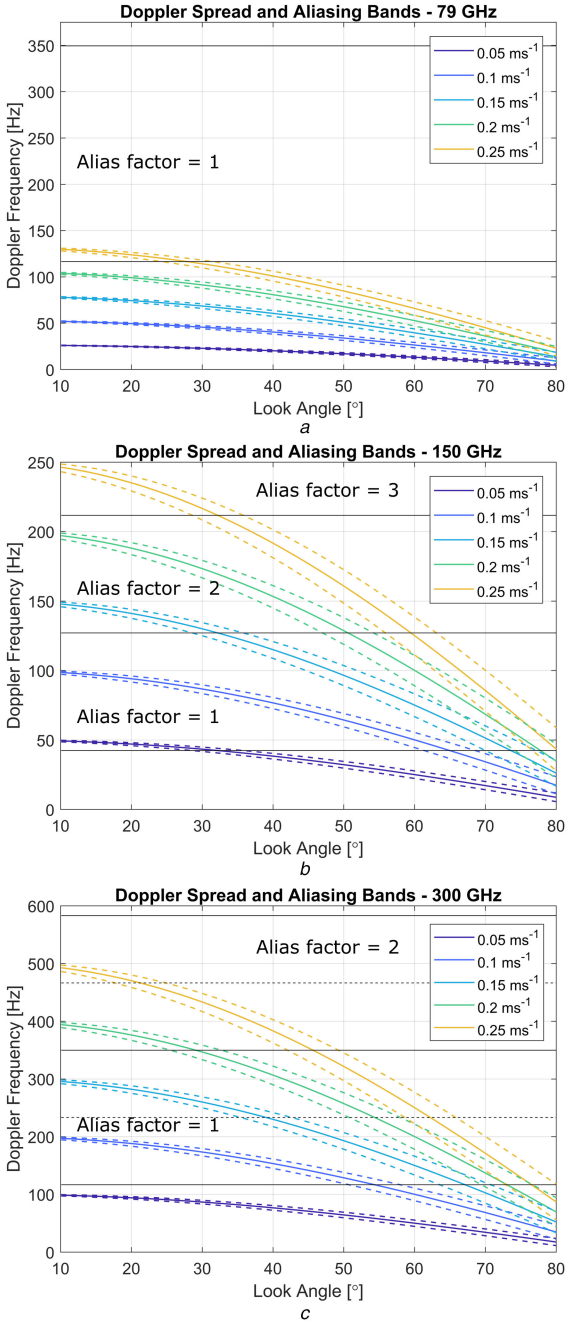

Fig. 5 *Doppler spread as a function of look angle at different platform velocities for three radar frequencies*
(a) 79 GHz, ***(b)*** 150 GHz, ***(c)*** 300 GHz. Black lines segregate Doppler aliasing bands governed by the chirp repetition rate of prototype experimental radar systems

A target cross-track range of 4.5 m was chosen to isolate target responses from other returns in the laboratory. The chosen experimental geometry gives an along-track beam width (which is essentially the un-refined along-track resolution) of 0.81, 0.79 and 0.76 m for the 79, 150, and 300 GHz radars, respectively. The difference is due to the relative positions of the radars on the radar platform, which also gives rise to a 0.2 m separation in along-track distance between each radar. As such the data must be temporally aligned to compensate for the difference in equivalent along-track positions of the radars. The target along-track distance was defined such that the 150 GHz radar beam centre meets the target centre at the mid-point of the linear trajectory.

4.3 Measurement overview and signal processing outline

Two types of measurements have been made, initially, corner reflectors were selected for reference targets due to their 'point-like' reflective nature. A set of experiments was conducted at 150 GHz to measure the Doppler spread across the beam width, test the application of DBS processing to localise the reflector positions in space and measure their separation. Secondly, measurements of actual complex targets were made at 79 and 300 GHz in order to investigate imaging through the use of azimuth refinement.

The general signal processing outline for DBS as applied to FMCW signals is as follows:

i. Fast-Fourier transform (FFT) baseband beat frequency signal to obtain *range profiles* (fast-time FFT)
ii. Form range profiles as a function of along-track platform displacement or, equivalently, chirp transmit time/number.
iii. FFT across range profiles over chirp integration time to obtain *range-Doppler* surface (slow-time FFT).
iv. Application of DBS mapping using (8) to transform Doppler to angle. This produces the *range-azimuth* surface.
v. Convert polar range-azimuth to a Cartesian x–y surface.

These processing steps will be illustrated in the next section.

Again for reasons of providing adequate azimuth refinement, the value of integration time for the processing was chosen to be 0.3 s – an along-track integration distance of 3 cm. This gives a refinement factor of 6 at 300 GHz (from (7)), giving a refined beamwidth of ∼1.2°. This is comparable to the two-way azimuthal beam width of the physical aperture imaging antennas mentioned in Section 4.1 and allows for azimuth scanned image comparisons.

5 Measurement results and analysis

5.1 Corner reflector localisation and separation measurement – 150 GHz

The plots in Fig. 6 show the measurement results for a single (left column) and two (right column) corner reflector targets. Plots in (Fig. 6*a*) show the radar range as a function of along-track distance (distance travelled along the linear positioner). Row (Fig. 6***b***) shows the spectrograms formed from the time history of the target bright points extracted from the range profiles. It should be noted that the along-track distance and time axes in Figs. 6*a* and *b* are simply related through the platform velocity.

It can be seen in the range plots that due to the beam width of the antennas, the corner reflector returns are spread out across the platform trajectory. The range of the target as a function of along-track distance corresponds to what would be expected from the experimental geometry. The shape of the spectrograms and the spread of Doppler frequencies during the motion (40–60 Hz) also correspond to what would be expected from the geometry and that calculated in Fig. 5*b*. In the two-target instance, it is obvious in both the range plot and spectrogram that the second reflector enters the beam first, as would be expected from its position and it is also angled more directly towards the radar, inferred from the much brighter return. It can be seen that there is a broadening in range spread, indicating the additional target is present and indeed in terms of range these two targets may be separable. This is especially so when considering the fine range resolution at low-THz frequencies; it is not possible to position both reflectors at the same range for the full radar trajectory. With such 'point-like' targets, at a conceptual level, it would be possible to localise the targets in azimuth purely by considering the positions of the peak magnitudes of the responses. Essentially the return power profile along the radar trajectory should follow the beam pattern shape; however, this is only possible in the simplest cases.

Fig. 6*c* shows range-Doppler surfaces for the single target and two targets, created at 10.8 s in the constant velocity section of the radar motion. The separation of the two targets (right circled) in the Doppler domain is clear. The plots of row (Fig. 6*d*) show the result of the DBS mapping. In the Cartesian x–y frame, the x-axis runs parallel to the direction of motion, the y-axis is perpendicular, (0, 0) is centred on the radar and the plot shows the plan view of the test scene. The circled bright points clearly show the localisation of the reflectors in Cartesian space at 10.8 s in the platform motion, calculation of the separation of the two target responses gives a value of 0.31 m, very close to the measured value of 0.3 m.

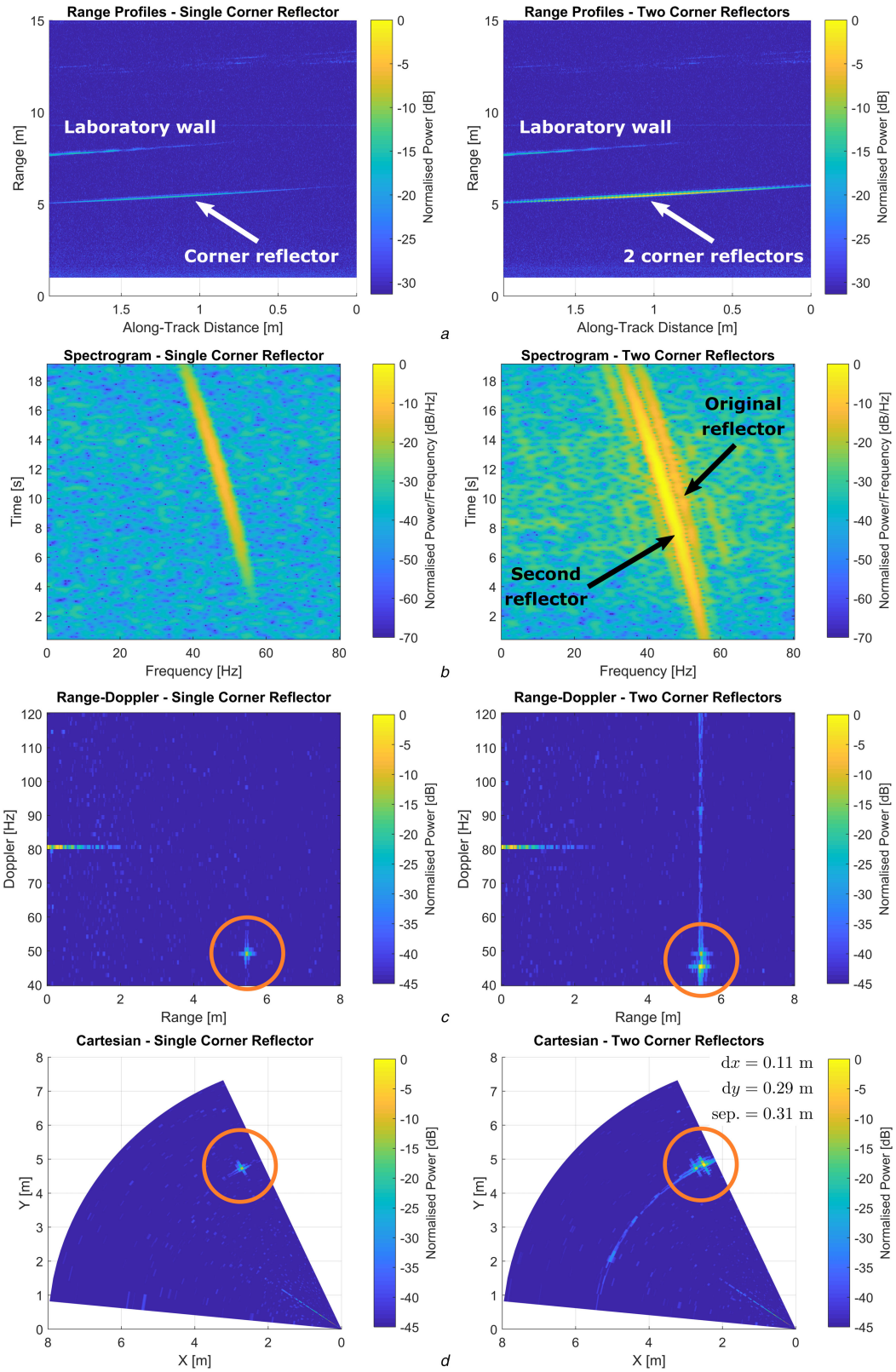

Fig. 6 *Measurement of single corner reflector target (left column) and two corner reflectors separated by 0.3 m (right column)*
(a) Shows radar range profiles as a function of the along-track distance of the radar platform, ***(b)*** Shows spectrograms formed from time history of reflector bright points extracted from the range profiles of (a), ***(c)*** Range-Doppler surfaces produced from range plots in (a), at 10.8 s into radar linear motion are shown, ***(d)*** Shows Cartesian plots localising corner reflector positions with respect to radar after application of DBS. Powers are normalised to the maximum target response within each sub-plot pair

5.2 DBS imaging of target objects at 79 and 300 GHz

Two complex targets were chosen on which to apply the DBS technique for imaging purposes. The first was a metallic trolley of dimension 1 m×0.5 m02150.5 m (L×W×H), the second was a bike of dimension 1.7 m×0.45 m×1 m; target objects are shown in Fig. 7*a*. The left column of the figure corresponds to the trolley and the right to the bike.

Fig. 7*b* shows the measured range profiles of the trolley and bike targets as a function of the radar along-track position at 79 GHz, Fig. 7*c* shows the equivalent at 300 GHz. The trolley occupies a range spread between 5 and 6.5 m approximately; as would be expected from its dimensions, the bike occupies a much narrower range spread. It should be emphasised that the range profile plots are in fact the raw wide antenna azimuth beam width

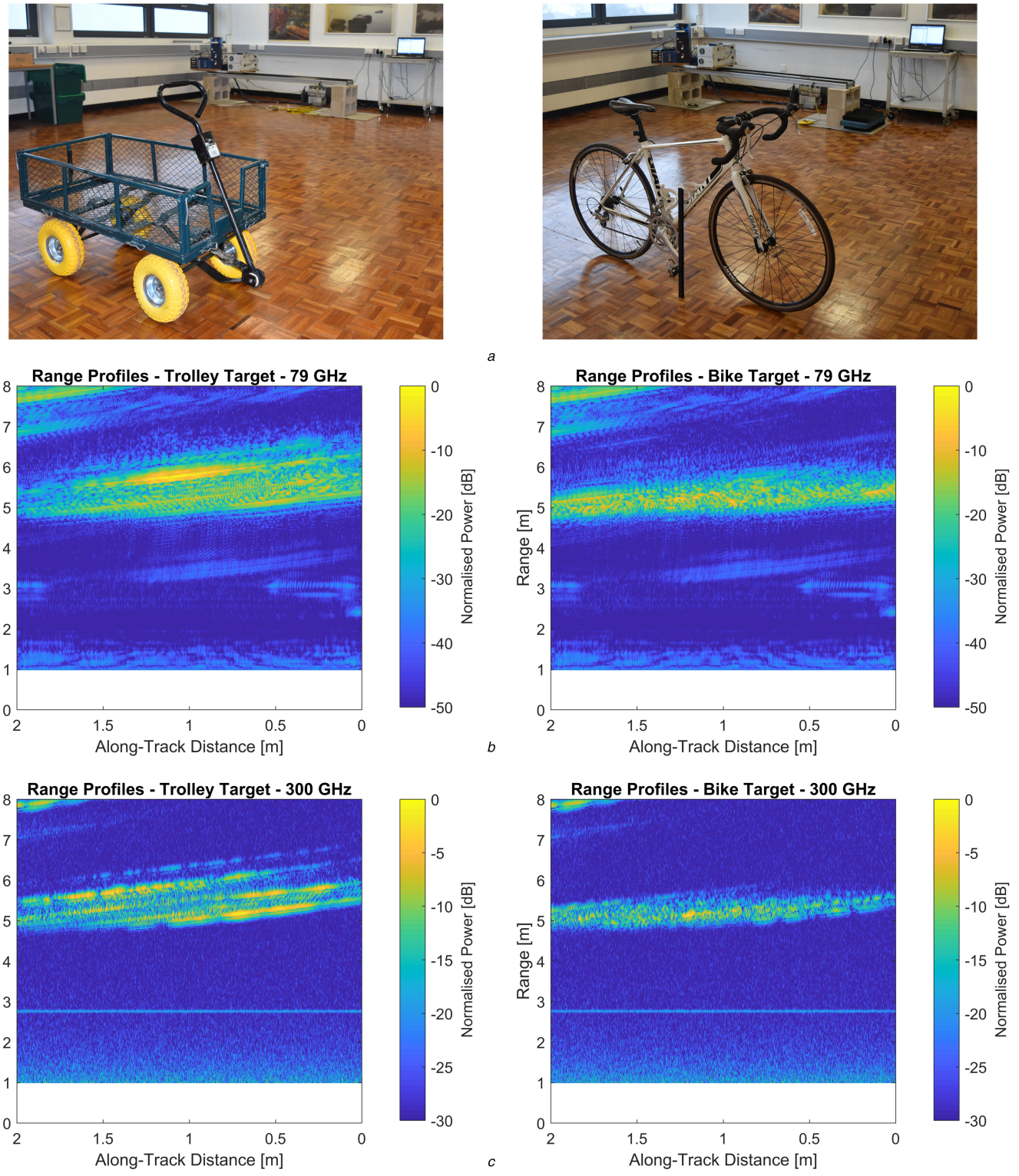

Fig. 7 *Target range profiles. Left column: trolley target, right column: bike target*

(a) Shows target positioned in front of the DBS measurement setup, ***(b)***, ***(c)*** Show range profiles as a function of the along-track distance of radar platform for 79 and 300 GHz, respectively. Target range profiles. Left column: trolley target, right column: bike target

target images and show no target detail apart from the range extents.

Applying the same processing as described in Section 4.3 and as performed on the corner reflector data of Section 5.1, the Doppler beam sharpened target images are presented in Fig. 8 – left column for trolley and right column for the bike. Fig. 8*a* (left) shows the trolley imaged (through DBS) at 79 GHz and Fig. 8*b* at 300 GHz, the comparative imaging improvement due to the use of a higher frequency is apparent. At 79 GHz, the target is localised to the correct position in the Cartesian plane and indeed the general size can be estimated. The 300 GHz image, however, allows the full rectangular shape and dimension of the target to be assessed and some details of the structure are apparent. The handle of the trolley may be seen as a separate bright point extending out from the main body in the *y*-dimension.

The same situation is seen for the bike target, the 79 GHz refined image in Fig. 8*a* (right), again indicates the general dimension of the object, and it is obviously smaller in extent than the trolley in the *y*-direction, as it should be. The 300 GHz sharpened image (Fig. 8*b*) shows the details of the front wheel, the handle bar extent and even an extended width region in the vicinity of the cranks/pedals/saddle (around 2 m in the *x*-direction). The full

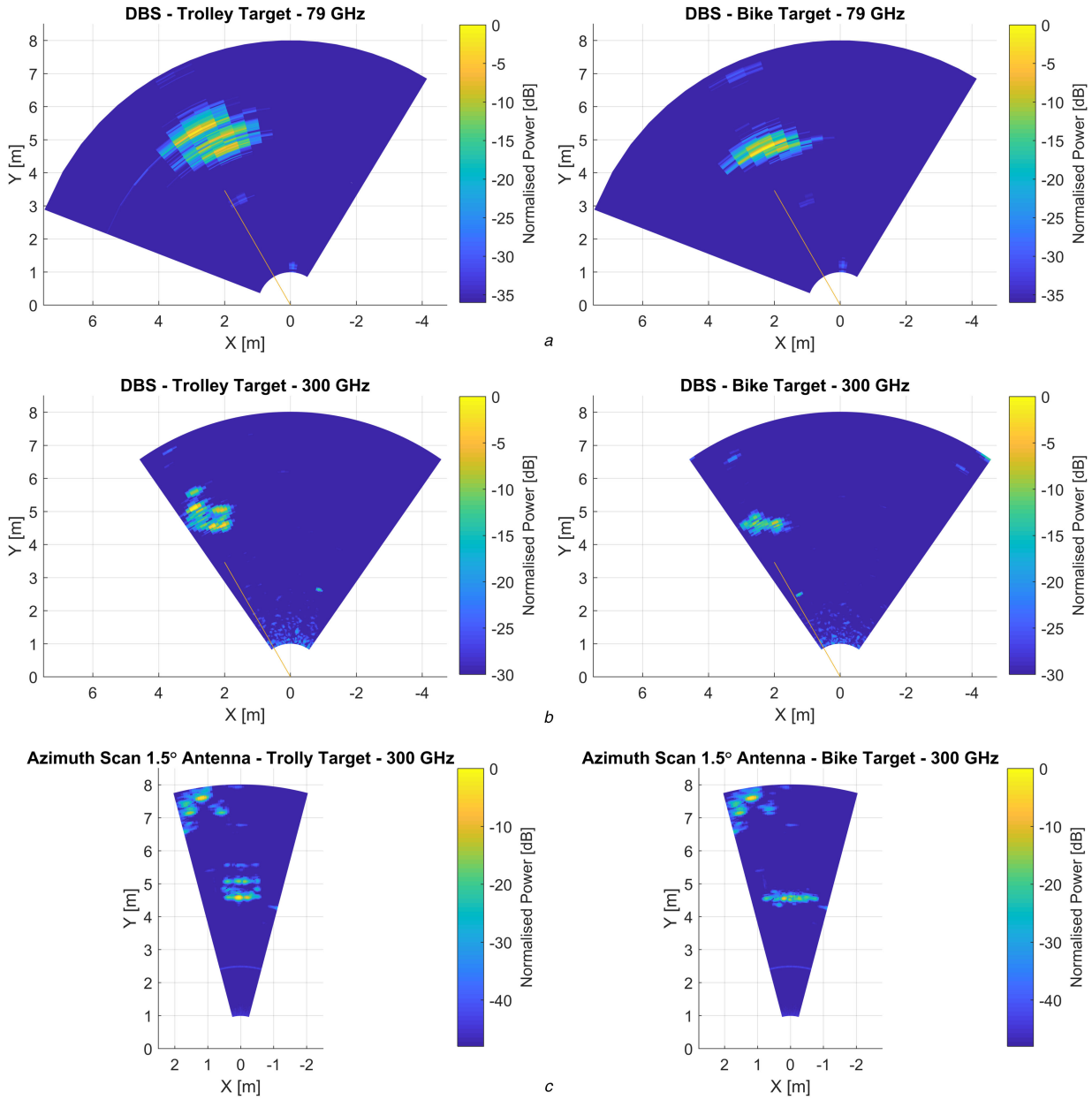

Fig. 8 *Target images. Left column: trolley target, right column: bike target*

(a), ***(b)*** Show trolley target images after application of DBS at 79 and 300 GHz, respectively. Orange line indicates antenna pointing, ***(c)*** Shows azimuth scanned 300 GHz images using 1.5° beamwidth imaging antennas. Powers are normalised to the maximum target response within each sub-plot pair

length of the bike, however, cannot be reconstructed in this experimental setup due to its length exceeding that of the along-track beam width (0.76 m) at 4.5 m cross-track range (reported in Section 4.2).

The images contained within Fig. 8*c* are azimuth scanned images of the two targets. These were produced by scanning the radar across the target with the 1.2° (two-way) azimuth beam width imaging antennas. The scan was incremental (step-by-step) and to draw a parallel with the DBS measurement, the radar dwelled for 0.3 s at each azimuth angle. In addition to this, as discussed in Section 4.3, the refined azimuth beamwidth for the 300 GHz DBS image is the same as the imaging antenna beamwidth used for the scanning. Again the full extent and shape of the objects are clear in the scanned images, and object features are visible, such as the bike handle bars. The exact replication of features between 300 GHz DBS and scanned images would not be expected as the illumination of the target is different in both cases, but nevertheless they appear to be very similar. The scanned images have higher definition whereas the DBS images appear slightly smeared, as may be expected due to the moving platform – this is a subject for further research related to the aspects of range/Doppler walk and integration time.

6 Conclusions and future plans

In this study, we have identified the potential for azimuth refinement using DBS at low-THz frequencies, applied to automotive/autonomous vehicle sensing. The improvements available have been demonstrated theoretically and it has been shown that low-THz frequencies are a must in order to achieve reasonable azimuth refinement in automotive scenarios. The refinement factors available under certain conditions give the potential for sub-degree synthetic beamwidths, something generally unobtainable with physical antennas and beamforming.

Experiments have been designed and carried out in order to test the application of DBS to low-THz measurement data. This was performed on both simple reference targets to assess the processing scheme, and then complex target objects to assess imaging capabilities. The DBS algorithm was successfully applied to localise the reference reflectors to the correct positions and allowed calculation of the separation of two reflectors. The imaging experiments highlighted the gains that can be made in image quality when moving from the current 79 GHz automotive band to prospective low-THz frequencies (300 GHz). It is the unique combination of low-THz DBS and the excellent range resolution at low-THz frequencies which allows such accurate localisation and

high-quality imaging. It was shown that a stationary (i.e. non-scanning) wide beam antenna mounted on a moving platform can deliver imagery at least comparable to that produced by physical beamforming – steering arrays or narrow beam scanning antennas as in the experimental case shown.

The experimental process brought to light considerations required regarding the experimental setup, e.g. consideration of Doppler aliasing with the prototype low-THz radar systems.

This is a first demonstration of the use of DBS at low-THz and further work will be focused on assessing and quantifying the actually achieved refinement – requiring further resolution experiments with reference reflectors. Image quality also requires some quantified assessment methodology. Another area of future research relates to the DBS processing and integration time. The integration time depends on many factors, such as target phase variation/scintillation with aspect angle, radar coherence time, range walk and Doppler walk/smearing – the characterisation of these factors at low-THz frequencies with large bandwidths is the subject for future research in this area. As DBS relies on platform motion, the combined effect of moving targets on the angular refinement will also be investigated. Real vehicular implementation would rely on the use of on-board sensors such as an IMU and global positioning system to determine the radar platform velocity, localisation, and orientation. The required accuracy of such sensors for motion compensation is also a subject for future research.

7 Acknowledgments

This work was supported by Jaguar Land Rover and the UK-EPSRC grants EP/N012372/1 and EP/N012240/1 as part of the jointly funded Towards Autonomy: Smart and Connected Control (TASCC) Programme.

8. References

[1] https://www.gov.uk/government/organisations/centre-for-connected-and-autonomous-vehicles

[2] ETSI EN 302 264-1.: 'Electromagnetic compatibility and radio spectrum matters (ERM); short range devices; road transport and traffic telematics (RTTT); short range radar equipment operating in the 77 GHz to 81 GHz band'. Available at http://www.etsi.org

[3] Sturm, C., Li, G, Lübbert, U.: '79 GHz automotive radar and its opportunities for frequency and bandwidth agile operation'. 2017 18th Int. Radar Symp. (IRS), Prague, 2017, pp. 1–6

[4] Jasteh, D., Hoare, E.G., Cherniakov, M., *et al.*: 'Experimental low-terahertz radar image analysis for automotive terrain sensing', *IEEE Geosci. Remote Sens. Lett.*, 2016, **13**, (4), pp. 490–494

[5] Stove, A.: 'Potential applications for low-tera-hertz radar'. 2015 16th Int. Radar Symp. (IRS), 2015, pp. 191–196

[6] Beckmann, P., Spizzichino, A.: '*The scattering of electromagnetic waves from rough surfaces*' (Artech house, Norwood, MA, 1987)

[7] Willetts, B., Gashinova, M., Stove, A., *et al.*: 'Low-THz rough surface imaging'. Proc. 13th European Radar Conf., London, UK, October 2016, pp. 394–397

[8] Waldschmidt, C., Meinel, H.: 'Future trends and directions in radar concerning the application for autonomous driving'. 2014 44th European Microwave Conf., Rome, 2014, pp. 1719–1722

[9] Balanis, C.A.: '*Advanced engineering electromagnetics*' (John Wiley, Hoboken, NJ, 2012, 2nd edn.)

[10] Bystrov, A., Hoare, E., Tran, T.Y., *et al.*: 'Automotive surface identification system based on modular neural network architecture'. 2017 18th Int. Radar Symp. (IRS), Prague, 2017, pp. 1–8

[11] Daniel, L., Phippen, D., Hoare, E., *et al.*: 'Multi-height radar images of road scenes at 150 GHz'. 2017 18th Int. Radar Symp. (IRS), Prague, 2017

[12] Liebe, H.J., Layton, D.H.: 'Millimeter-wave properties of the atmosphere: laboratory studies and propagation modelling', NTIA Report 87–224, U.S. Department of Commerce

[13] Recommendation ITU-R P.838–3.: 'Specific atenuation model for rain use in prediction methods'

[14] Ishii, S., Kinugawa, M., Wakiyama, S., *et al.*: 'Rain attenuation in the microwave-to-terahertz waveband', *Wirel. Eng. Technol.*, 2016, **7**, pp. 59–66, doi: 10.4236/wet.2016.72006

[15] Daniel, L., Phippen, D., Hoare, E., *et al.*: 'Low-THz radar, lidar and optical imaging through artificially generated fog'. Int. Conf. on Radar Systems (Radar 2017), Belfast, 2017, pp. 1–4

[16] Wiley, C.A.: 'Synthetic aperture radars', *IEEE Trans. Aerosp. Electron. Syst.*, 1985, **AES-21**, (3), pp. 440–443

[17] Sun, H., Liu, G., Gu, H., *et al.*: 'The development of DBS imaging based on airborne pulse Doppler radar in China', *Microw. J.*, 2001, Available at http://www.microwavejournal.com/articles/3143-the-development-of-dbs-imaging-based-on-airborne-pulse-doppler-radar-in-china

[18] Chen, H., Li, M., Wang, Z., *et al.*: 'Super-resolution Doppler beam sharpening imaging via sparse representation', *IET Radar, Sonar Navig.*, 2016, **10**, (3), pp. 442–448

[19] Yang, H., Mao, D., Zhang, Y., *et al.*: 'Doppler beam sharpening imaging based on fast iterative adaptive approach'. 2017 IEEE Radar Conf. (RadarConf), 2017, pp. 1419–1423

[20] Qi, L., Zheng, M., Yu, W., *et al.*: 'Super-resolution Doppler beam sharpening imaging based on an iterative adaptive approach', *Remote Sens. Lett.*, 2016, **7**, (3), pp. 259–268

[21] Laribi, A., Hahn, M., Dickmann, J., *et al.*: 'A new height-estimation method using FMCW radar Doppler beam sharpening'. 2017 25th European Signal Processing Conf. (EUSIPCO), Kos, 2017, pp. 1932–1936

[22] Li, J., Stoica, P.: 'Efficient mixed-spectrum estimation with applications to target feature extraction', *IEEE Trans. Signal Process.*, 1996, **44**, (2), pp. 281–295

[23] Tait, P.: '*Introduction to radar target recognition*' (IET, London, 2005)

[24] Skolnik, M.J.: '*Radar handbook*' (McGraw-Hill, New York, NY, 2008, 3rd edn.)

[25] Bosch MMR: Available at https://www.bosch-mobility-solutions.com/en/products-and-services/passenger-cars-and-light-commercial-vehicles/driver-assistance-systems/predictive-emergency-braking-system/mid-range-radar-sensor-(mrr)/

[26] Slocum, D.M., Slingerland, E.J., Giles, R.H., *et al.*: 'Atmospheric absorption of terahertz radiation and water vapor continuum effects', *J. Quant. Spectrosc. Radiat. Transfer*, 2013, **127**, pp. 49–63

[27] IEEE Connected Vechicles. Available at http://sites.ieee.org/connected-vehicles/

[28] Tian, J., Wei, C., Lin, M., *et al.*: 'DBS imaging based on keystone transform', *J. Syst. Eng. Electron.*, 2012, **23**, pp. 342–348, 10.1109/JSEE.2012.00042

[29] Song, X.Y., Li, Z.F., Bao, Z.: 'High squint DBS imaging', *Mod. Rad.*, 2004, **26**, pp. 30–33

[30] Phippen, D., Daniel, L., Gashinova, M., *et al.*: 'Trilateration of targets using a 300 GHz radar system'. Int. Conf. on Radar systems 2017 (Radar 2017), Belfast, 2017